Molecular Vision 2018; 24:353-366 <http://www.molvis.org/molvis/v24/353>
Received 31 August 2017 | Accepted 16 May 2018 | Published 18 May 2018

Subtle thinning of retinal layers without overt vascular and inflammatory alterations in a rat model of prediabetes

Mariana R. P. Alves,[1,2] Raquel Boia,[1,2] Elisa J. Campos,[1,2] João Martins,[1,2] Sara Nunes,[1,2] Maria H. Madeira,[1,2] Ana Raquel Santiago,[1,2,3] Frederico C. Pereira,[1,2] Flávio Reis,[1,2] António F. Ambrósio,[1,2,3] Filipa I. Baptista[1,2]

[1]Coimbra Institute for Clinical and Biomedical Research (iCBR), Faculty of Medicine, University of Coimbra, Coimbra, Portugal; [2]CNC.IBILI Consortium, University of Coimbra, Coimbra, Portugal; [3]Association for Innovation and Biomedical Research on Light (AIBILI), Coimbra, Portugal

Purpose: Diabetic retinopathy is a neurovascular disease characterized by increased permeability of the blood–retinal barrier, changes in the neural components of the retina, and low-grade chronic inflammation. Diabetic retinopathy is a major complication of diabetes; however, the impact of a prediabetic state on the retina remains to be elucidated. The aim of this study was to assess possible early retinal changes in prediabetic rats, by evaluating changes in the integrity of the blood–retinal barrier, the retinal structure, neural markers, and inflammatory mediators.

Methods: Several parameters were analyzed in the retinas of Wistar rats that drank high sucrose (HSu; 35% sucrose solution during 9 weeks, the prediabetic animal model) and were compared with those of age-matched controls. The permeability of the blood–retinal barrier was assessed with the Evans blue assay, and the content of the tight junction proteins and neural markers with western blotting. Optical coherence tomography was used to evaluate retinal thickness. Cell loss at the ganglion cell layer was assessed with terminal deoxynucleotidyl transferase (TdT) dUTP nick-end labeling (TUNEL) assay and by evaluating the immunoreactivity of the Brn3a transcription factor. To assess retinal neuroinflammation, the mRNA expression and protein levels of inducible nitric oxide synthase isoform (iNOS), interleukin-1 beta (IL-1β), and tumor necrosis factor (TNF) were evaluated. Iba1 and MHC-II immunoreactivity and translocator protein (TSPO) mRNA levels were assessed to study the microglial number and activation state.

Results: The thickness of the inner retinal layers of the HSu-treated animals decreased. Nevertheless, no apoptotic cells were observed, and no changes in retinal neural markers were detected in the retinas of the HSu-treated animals. No changes were detected in the permeability of the blood–retinal barrier, as well as the tight junction protein content between the HSu-treated rats and the controls. In addition, the inflammatory parameters remained unchanged in the retina despite the tendency for an increase in the number of retinal microglial cells.

Conclusions: In a prediabetic rat model, the retinal structure is affected by the thinning of the inner layers, without overt vascular and inflammatory alterations. The results suggest neuronal dysfunction (thinning of the inner retina) that may precede or anticipate the vascular and inflammatory changes. Subtle structural changes might be viewed as early disturbances in an evolving disease, suggesting that preventive strategies (such as the modification of diet habits) could be applied at this stage, before the progression toward irreversible dysfunction and damage to the retina.

Diabetes mellitus often induces ophthalmic complications in patients, as diabetic retinopathy is the most frequent and potentially the most blinding complication [1]. This neurovascular disease is most characterized by the breakdown of the blood–retinal barrier (BRB) and the changes in its permeability [2]. Additional pathology includes alterations to the neural components of the retina and retinal neuroinflammation [3].

Correspondence to: Filipa I. Baptista, Coimbra Institute for Clinical and Biomedical Research (iCBR), Faculty of Medicine, University of Coimbra, Azinhaga de Santa Comba 3004-548 Coimbra, Portugal; Phone: +351239480235; email: fibaptista@fmed.uc.pt
Dr. Alves is now at Developmental Biology Unit, European Molecular Biology Laboratory, Meyerhofstrasse 1, 69117 Heidelberg, Germany; Martins J. is now at CIBIT/ICNAS - Institute of Nuclear Sciences Applied to Health, University of Coimbra.

Although diabetic retinopathy is recognized as a vascular disease, a large body of evidence shows that retinal neurodegeneration also occurs [4]. It was suggested that changes in vascular permeability may be due to alterations in the neural retina, inducing a disruption of the communication between neurons and glial and endothelial cells [5]. Impairments detected in electroretinograms performed in animals and diabetic patients, as well as alterations in color and contrast sensitivity [6,7], demonstrate that this pathology also affects retinal neurons [3]. Diabetic patients present a thinning of the nerve fiber layer, suggesting a loss of retinal ganglion cells (RGCs) [4]. Diabetes also has an impacts on retina neurotransmission [8], altering the levels of retinal ionotropic glutamate receptor subunits in an animal model of diabetes [9,10] and changing the levels of several synaptic [11] and motor proteins [12]. These effects may consequently underlie visual impairments in diabetic retinopathy.

Additionally, diabetes exhibits features of a low-grade chronic inflammatory pathology [4], with changes in genes associated with retinal inflammatory processes [13]. These alterations occur in conjunction with an increase in apoptosis and retinal vascular permeability [13]. In the retinas of diabetic animals [14] and humans [15], proinflammatory mediators are released by resident immune microglial cells. In addition, an increased number of hyperreflective spots, which suggest aggregates of activated microglia, have been observed in patients with diabetic retinopathy with spectral domain optical coherence tomography (SD-OCT) [16]. The involvement of neuroinflammation in the development of diabetic retinopathy has been recently reviewed [17].

Prediabetes (also called intermediate hyperglycemia) is a metabolic impairment defined by glycemic variables lower than diabetes but higher than normoglycemia, and is recognized as a high-risk condition for the development of diabetes [18]. Before overt type 2 diabetes (T2D), a prediabetic state can be identified by impaired fasting glucose (IFG) or impaired glucose tolerance (IGT) using an oral glucose tolerance test (OGTT). The advancement from early metabolic changes that precede diabetes, such as IGT and/or IFG, to a diabetic state can take several years [19,20]; however, the majority of patients in prediabetic states will ultimately develop diabetes [21].

Little is known regarding the impact of intermediate hyperglycemia on the retina; however, changes in the retina may be present before a diabetes diagnosis [3]. Moreover, early stage identification of retinal abnormalities in prediabetic/insulin-resistant patients may be an adequate strategy to diagnose, accompany, and thus, prevent the disease progression to more advanced and serious stages of the disease. Therefore, the aim of this work was to identify potential early structural, molecular, and cellular retinal changes, in a prediabetic rat model, by evaluating BRB integrity and neural and inflammatory markers.

To elucidate whether the initial stages of retinal dysfunction are already present in an early stage of insulin resistance, we used a prediabetes rat model. This animal model is induced by a high sucrose (HSu) diet and is characterized by the presence of IGT, accompanied by fasting normoglycemia, hyperinsulinemia, insulin resistance, together with hypertriglyceridemia [19,22,23].

METHODS

Animals: Male Wistar rats aged 16 weeks (Charles River Laboratories, Lyon, France) were housed in certified facilities, in a temperature- and humidity-controlled environment under a 12h:12 h light-dark cycle. Animals were provided with a standard rodent diet ad libitum and were randomly divided into two groups: rats that received 35% sucrose in drinking water for 9 weeks (high sucrose, HSu), as previously described [19] and the age-matched control group (water).

Evaluation of metabolic and biochemical parameters was performed as previously described [19,22]. All procedures involving animals were performed in agreement with the EU Directive 2010/63/EU for animal experiments, and in accordance with the Association for Research in Vision and Ophthalmology (ARVO) statement for the use of animals in ophthalmic and vision research.

Preparation of total retinal extracts and western blotting analysis: The preparation of the total retinal extracts and western blotting analysis was performed as previously described [12]. Primary antibodies used are listed in Table 1. After protein detection, the membranes were reprobed for β-actin immunoreactivity (1:5,000; Sigma, St. Louis, MO) as a loading control.

Terminal Transferase dUTP Nick End Labeling (TUNEL) staining.: Retinal cells undergoing apoptosis were identified by TUNEL assay in retinal cryosections using the DeadEnd Fluorimetric TUNEL system (Promega Corporation, WI) as previously described [24]. Cells were stained with DAPI to label the nuclei. The images were acquired with a fluorescence microscope (Axio HXP 120, Zeiss, Oberkochen, Germany).

Assessment of BRB permeability using Evans blue dye: Retinal blood vessel permeability was evaluated using Evans blue dye, following the procedure previously described [25,26]. Evans blue binds tightly to serum albumin, which crosses the BRB when its permeability is affected. Evans blue (100 mg/ml; Sigma) was dissolved in PBS (in mM: 137 NaCl, 2.7 KCl, 10 Na_2HPO_4, 1.8 KH_2PO_4; pH 7.4), sonicated for 20 min, and filtered (pore size, 0.2 µm).

HSu-treated rats and age-matched controls were anesthetized with an intraperitoneal injection of ketamine (50 mg/kg bodyweight; Imalgene 1000, Merial, Lyon, France) and xylazine (10 mg/kg bodyweight; Rompum®, Bayer, Leverkusen, Germany), and Evans blue dye (100 mg/kg bodyweight) was injected using a 30-gauge needle through the tail vein, previously warmed up using a heating lamp. Additional anesthesia (ketamine, 50 mg/kg bodyweight) was provided during the procedure, if needed. Animals were kept warm during the procedure. After the dye circulated for 120 min, the chest cavity was opened, and the animals were perfused via the left ventricle, with 1% paraformaldehyde (PFA) in 50 mM citrate buffer (pH 4.2, 37 °C; about 56 ml) to clear the dye from the vessels. Immediately following perfusion, the eyes

Table 1. List of primary antibodies used.

Primary antibody	Sample	Antibody dilution	Protein (µg)	Source
Mouse anti-Vimentin	Total Extracts Retina	1:5000	10	Thermo Scientific
	Immunohistochemistry	1:200	-	Thermo Scientific
Rabbit anti-Occludin	Total Extracts Retina	1:250	20	Invitrogen
Mouse anti-iNOS	Total Extracts Retina	1:500	40	Abcam
Rabbit anti-Claudin-5	Total Extracts Retina	1:250	10	Invitrogen
Rabbit anti-TUJ-1	Total Extracts Retina	1:2500	10	Abcam
	Immunohistochemistry	1:1000	-	Abcam
Rabbit anti-Actin	Total Extracts Retina	1:5000	10	Sigma
Mouse anti-GFAP	Total Extracts Retina	1:5000	10	Calbiochem
	Immunohistochemistry	1:500	-	Calbiochem
Mouse anti-synaptophysin	Total Extracts Retina	1:1000	10	Sigma
	Immunohistochemistry	1:200	-	Sigma
Rabbit anti-ZO-1	Total Extracts Retina	1:250	40	Invitrogen
Rabbit anti-Iba-1	Immunohistochemistry	1:1000	_	Wako
Mouse anti-MHC-II	Immunohistochemistry	1:200	_	AbD Serotec

were enucleated, and the retinas were carefully dissected under an operating microscope and rinsed in PBS. Retinas were thoroughly dried in a Speed-Vac (5 h, with heating), and the dry weight of each retina was measured. Albumin leakage into the retina was assessed via measurement of the extravasated Evans blue dye. This dye was extracted by incubating each retina in 110 µl formamide for 18 h at 70 °C with gentle shaking. The extract was ultracentrifuged (TL-100, Beckman, CA) at a speed of 200,000 ×*g* for 45 min, at 4 °C. The absorbance of supernatant (50 µl) was measured in a spectrophotometer (Synergy HT, BioTek, Winooski, VT) at 620 nm absorbance (maximum) and 740 nm absorbance (minimum). The concentration of the dye in the samples was calculated from a standard curve (100–5,000 ng/ml) of Evans blue dye in formamide and normalized to the dry retinal weight.

Optical coherence tomography: The structural changes in the retina were evaluated in vivo with SD-OCT (Phoenix Micron IV, Phoenix Research Labs, Pleasanton, CA). The animals were anesthetized with an intraperitoneal injection of ketamine (75 mg/kg bodyweight) and xylazine (10 mg/kg bodyweight). The data were collected from both eyes after corneal anesthesia with topical 4 mg/ml oxybuprocaine hydrochloride (Anestocil®, Laboratório Edol, Carnaxide, Portugal) and pupil dilation with topical 10 mg/ml tropicamide (Tropicil®, Laboratório Edol). As the OCT technique includes the contact of a lens with the animal eye, we used topical oxybuprocaine to obtain ocular analgesia, in addition to the animal anesthesia. This procedure was adopted to minimize pain and improve animal welfare. To our knowledge, this procedure does not affect the structural parameters assessed by OCT. The cornea was kept hydrated and optically cleared with hydroxypropyl methylcellulose (Methocel™ 2%, Dávi II – Farmacêutica S.A., Barcarena, Portugal) during the whole procedure. The SD-OCT system used was able to capture 10,000–20,000 A scans per second with an axial resolution of 2 µm and a transverse resolution of 4 µm. For each eye, 13 tomographic images, obtained from line scans, plus the respective fundus of the eye, were acquired. The first image was acquired centered on the optic nerve head, followed by six scans above and six scans beneath that reference. In this way, in total, a 1,700 µm high region in the retina was scanned.

Tomographic images were analyzed using the segmentation software InSight (Phoenix Research Labs). Four layers in the retina were considered: (1) the ganglion cell layer (GCL), the retinal nerve fiber layer (RNFL), and the inner plexiform layer (IPL), between the inner limiting membrane (ILM) and the interface IPL-inner nuclear layer (INL); (2) the INL, between the interface of the IPL and the INL and the outer plexiform layer (OPL); (3) the outer nuclear layer (ONL), between the OPL and the outer limiting membrane (OLM); and (4) the inner segments (IS) and the outer segments (OS), between the OLM and the RPE.

Preparation of retinal cryosections and immunohistochemistry: The preparation of the retinal cryosections (16 µm) and immunohistochemistry were performed as previously

Table 2. Primer sequences.

Gene	Forward primer (5′-3′)	Reverse primer (5′-3′)	Amplicon size (bp)
Reference genes			
Hprt	ATGGGAGGCCATCACATTGT	ATGTAATCCAGCAGGTCAGCAA	77
Ywhaz	CAAGCATACCAAGAAGCATTTGA	GGGCCAGACCCAGTCTGA	76
Rho	GCAACAGGAGTCGGCTACCA	GCATAGGGAAGCCAGCAGATC	76
Target genes			
Tnf	CCCAATCTGTGTCCTTCT	TTCTGAGCATCGTAGTTGT	90
Il-1β	ATAGAAGTCAAGACCAAAGTG	GACCATTGCTGTTTCCTAG	109
NOS2	AGAGACAGAAGTGCGATC	AGATTCAGTAGTCCACAATAGTA	96
Pou4fi	ACCCTGTTCGTTTCAAATAG	AGCGTTTATCCCTGGTAAT	104
Tspo	TGTATTCGGCCATGGGGTATG	GAGCCAGCTGACCAGTGTAG	105
Qualitative PCR			
Actb	GCTCCTCCTGAGCGCAAG	CATCTGCTGGAAGGTGGACA	75

described [12]. Primary antibodies used in immunohistochemistry are listed in Table 1.

Image acquisition and analysis: Sections were observed with a fluorescence microscope (Axio HXP 120, Zeiss, Oberkochen, Germany), using an LD Plan-Neofluar 40x/0.6 Korr Ph2 M27 objective. For the analysis of neuronal, macroglial, and microglial cell markers, slides containing retinal slices from the control and HSu groups were blind coded and captured under the same conditions (four retinal sections per animal were used for quantification). In each image, the number of cells stained with 4',6-diamidino-2-phenylindole (DAPI; ganglion/displaced amacrine cells – DAPI-positive cells at the GCL), the number of Brn3a (RGCs) immunoreactive cells, or the number of cells immunoreactive to Iba1 (Iba1-positive cells) was counted, and the results were expressed per millimeters of the retina. Representative images were acquired using a laser scanning confocal microscope LSM 710 META (Zeiss).

RNA extraction and reverse transcription: Total RNA was isolated from the rat retinas using TRIzol reagent (Invitrogen, Life Technologies, Carlsbad, CA). RNA samples were dissolved in 16 µl of Milli-Q water, and the concentration and purity of the total RNA were determined using NanoDrop ND1000 (Thermo Scientific, Waltham, MA). Resulting RNA samples were treated with DNase I (DNase I; amplification grade, Invitrogen, Life Technologies) to eliminate possible contamination with genomic DNA. Total RNA (1 µg) was reversed transcribed according to the instructions provided by the manufacturer (NZYTech, Lisbon, Portugal). The resultant cDNA was treated with RNase-H for 20 min at 37 °C. For all cDNA samples, a 1:2 dilution was prepared, and the samples were stored at −20 °C until quantitative PCR (qPCR) analysis. Genomic DNA contamination was evaluated with conventional PCR for β-actin using intron-spanning primers (Table 2), as previously described [24].

Real-time quantitative PCR: qPCR was performed using StepOnePlus (Applied Biosystems, Foster City, CA) based on the real-time monitoring of fluorescent SYBR Green. The PCR conditions were as follows: iTaq™ Universal SYBR® Green Supermix (Bio-Rad, Hercules, CA), 200 nM primers (Table 2), and 2 µl of 1:2 dilution cDNA, in a total volume of 20 µl. Cycling conditions were a melting step at 95 °C for 15 s, annealing-elongation at 60 °C for 45 s, and extension at 72 °C for 30 s, with 40 cycles. A dissociation curve at the end of the PCR run was performed by ramping the temperature of the sample from 60 °C to 95 °C, while continuously collecting fluorescence data. Ct values were converted to "Relative quantification" using the 2^(-ΔΔCt) method previously described [27]. *Hprt*, *Ywhaz*, and *rhodopsin* were evaluated as housekeeping genes using NormFinder Add In for Microsoft Excel [28]. Because *Hprt* was the most stable gene in all conditions, it was used as the reference gene.

Enzyme-linked immunosorbent assay: Quantification of the interleukin-1β beta (IL-1β) and tumor necrosis factor (TNF) protein levels was performed with enzyme-linked immunosorbent assay (ELISA), as previously described [24]. The protein concentration of each sample was determined by the bicinchoninic acid protein assay according to the manufacturer's instructions (Pierce Biotechnology, Waltham, MA). The cytokine concentration of each sample was normalized to the total protein concentration.

Statistical analysis: The results are presented as mean ± standard error of the mean (SEM). Statistical analysis was performed in Prism 5.03 Software for Windows (GraphPad

Table 3. Metabolic and biochemical data of control and HSu groups for 9 weeks.

Parameters	Control	HSu
Bodyweight (g)	486.50±16.70	496.67±11.83
Glycemic profile		
Postprandial glycemia (mg/dl)	200.00±7.87	245.00±8.38**
Fasting glycemia (mg/dl)	96.81±1.72	101.64±1.24
Glucose AUC-GTT (mg/dl/120 min)	29,209.17±2429.31	43,438.60±3905.57*
HbA1c (%)	3.78±0.037	3.9±0.045
Insulinemic profile and insulin resistance		
Fasting insulin (µg/l)	2.03±0.18	2.59±0.61
HOMA-IR ($x10^{-5}$)	1.40±0.14	2.47±0.35*
Glucose ITT 0 min (mg/dl)	108.20±4.74	118.00±2.47
Glucose ITT 15 min (mg/dl)	97.50±6.61	122.20±6.91*
Glucose ITT 30 min (mg/dl)	78.17±2.0	91.50±4.06*
Glucose ITT 45 min (mg/dl)	75.17±3.79	87.83±3.18*
Glucose ITT 60 min (mg/dl)	67.00±4.83	75.67±6.92
Glucose ITT 120 min (mg/dl)	65.33±6.90	90.5±11.55
Lipid profile		
Total-Cholesterol (mg/dl)	61.50±3.15	60.83±4.80
Triglycerides (mg/dl)	146.70±17.84	235.3±38.87*

Data are expressed as mean ± SEM, *p<0.05; **p<0.01 versus the Control group (n=5/6). AUC, area under the curve; GTT, glucose tolerance test; HbA1c, glycated hemoglobina; HOMA-IR, Homeostatic Model Assessment for Insulin Resistance; ITT, insulin tolerance test.

Software, Inc.). The normality of the data was assessed with Shapiro-Wilk and Kolmogorov–Smirnov normality tests. Accordingly, data were analyzed with a non-parametric Mann–Whitney test. Differences with a p value of less than 0.05 were considerably statistically significant.

RESULTS

Evaluation of bodyweight and metabolic and biochemical parameters: The intake of 35% sucrose for 9 weeks did not affect the bodyweight of the HSu-treated rats when compared to that of the control animals (Table 3). Regarding the glycemic profile, there were no differences in plasma glucose levels between the HSu-treated rats in fasted states compared to the control animals. However, a statistically significant increase in plasma glucose levels in the postprandial state in the HSu rats was found. In addition, high sucrose consumption resulted in reduced glucose tolerance, as the recovery of glucose levels to basal levels was slower compared to the control animals, confirmed by the area under the curve (AUC) of the GTT (Table 3). Simultaneously, there was an impairment in insulin response after 9 weeks of sucrose intake, as confirmed by the insulin tolerance test (ITT). In this test, after the insulin injection, the reduction of blood glucose levels was slower in the HSu rats, revealing a reduced sensitivity to insulin. Moreover, the HOMA-IR (Homeostatic Model Assessment for Insulin Resistance) index, an additional measure of insulin resistance, was statistically significantly higher in the HSu rats compared with the controls.

Concerning the lipid profile, no changes were found in the total cholesterol levels between the two groups of animals, but the HSu-treated animals presented higher levels of triglycerides. Overall, these metabolic and biochemical data (Table 3) are in accordance with previous data obtained in the same prediabetic animal model [19,22]: IGT, fasting normoglycemia, hyperinsulinemia, insulin resistance, and hypertriglyceridemia.

Tight junction proteins and BRB permeability are not affected in the retinas of HSu-treated rats: Increased BRB permeability in diabetic animals is associated with changes in the content and distribution of tight junction proteins in retinal vessels [29,30]. Claudins, occludin, and zonula occludens-1 (ZO-1) are crucial determinants of BRB permeability [29]. BRB permeability was assessed using the Evans blue dye assay. Non-statistically significant changes were found in BRB permeability. Evans blue accumulation in the retina was not statistically significantly different between the two groups of animals (9.26±1.19 µg Evans blue/g retina versus 10.51±1.98 µg Evans blue/g retina, for HSu-treated and control

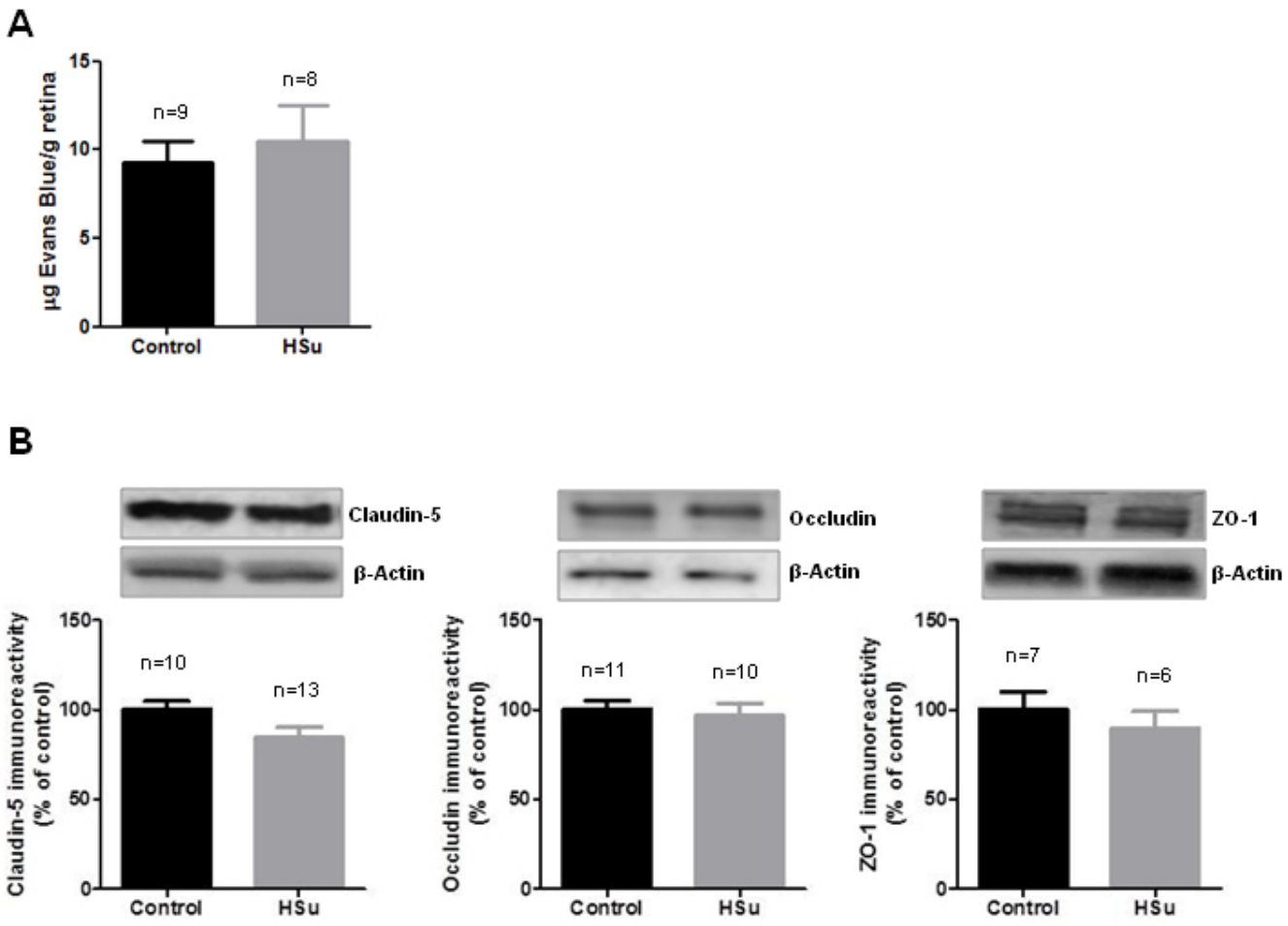

Figure 1. Chronic HSu treatment does not affect tight junction proteins and BRB permeability in the retina. **A**: The permeability of the blood–retinal barrier (BRB) was assessed with the Evans blue dye method. The results are expressed as milligrams of Evans blue per grams of retina, and are presented as mean ± standard error of the mean (SEM). **B**: The content of tight junction proteins (claudin-5, occludin, and ZO-1) were analyzed with western blotting in total retinal extracts obtained from control and high sucrose (HSu)-treated animals. Representative images of immunoreactive protein bands are presented above the graphs, as well as the respective loading control (β-actin). The results are expressed as a percentage of the age-matched controls, and data are presented as mean ± SEM.

animals, respectively; Figure 1A). The content of claudin-5, occludin, and ZO-1 in the retina was evaluated with western blotting. No statistically significant alterations were found in the HSu-treated animals compared with the controls (Figure 1B). These results indicate that at this early stage of insulin resistance the integrity of the BRB is not affected.

HSu diet induces retinal thinning: Diabetes is also characterized by structural changes in the neural retina. However, to our knowledge, it is unknown whether these alterations are already present in a prediabetic state. SD-OCT was used to analyze, noninvasively, the thickness of retinal layers in vivo (Figure 2A). After 9 weeks of the HSu diet, there was a subtle, but statistically significant, thinning of several retinal layers, particularly the RNFL, GCL, and IPL and the INL (Figure 2B).

It has been demonstrated that neuronal cells of the retina, namely, RGCs, are affected by diabetes [31-33]. In the HSu model, despite the thinning of the RNFL, GCL, and IPL, no changes in the number of cells (DAPI-positive cells) were observed in the GCL (Figure 2C). In addition, no apoptotic cells (terminal deoxynucleotidyl transferase (TdT) dUTP nick-End labeling (TUNEL)-positive cells) were detected in the retinas of the HSu-treated rats (Figure 2D). The impact of the HSu diet on RGCs was further studied with the evaluation of the Brn3a transcription factor that is expressed only in RGCs in the retina [34]. There was no alteration in the

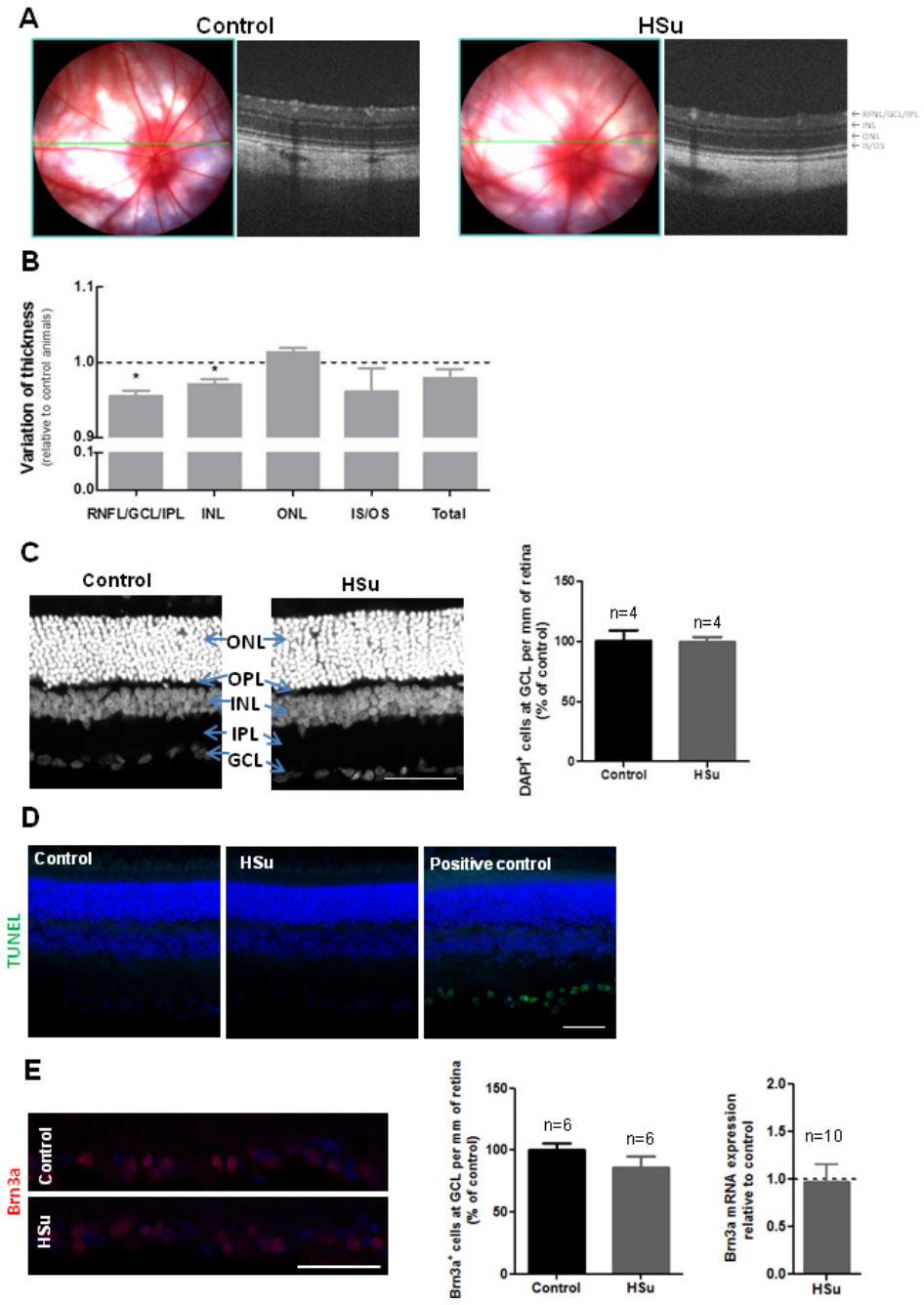

Figure 2. High sucrose diet induces a decrease in retinal thickness. **A**: Representative fundus image of a rat eye showing the line scan (green line) and the corresponding retinal tomographic images. Retinal thickness was assessed in optical coherence tomography (OCT) images obtained from different bright-field eye fundus scans. **B**: Retinal tomographic images obtained from the linear scans were used to evaluate the thickness of the retinal layers (the retinal nerve fiber layer (RNFL), the ganglion cell layer (GCL), and the inner plexiform layer (IPL), the inner nuclear layer (INL), the outer nuclear layer (ONL), the inner segments (IS) and the outer segments (OS), and the total) from control and high sucrose (HSu)-treated animals. Data are expressed as a variation in the retinal thickness of the HSu-treated animals relative to the control animals and are presented as the mean ± standard error of the mean (SEM) of four to six animals. *p<0.05 statistically significantly different from the respective age-matched control. **C**: Nuclei were stained with 4',6-diamidino-2-phenylindole (DAPI), and the number of DAPI-positive cells in the GCL was counted. Results are presented as the number of DAPI-positive cells per millimeter of retina and represent the mean fold change of the control ± SEM. Scale bar: 50 µm. **D**: Cell death was evaluated with terminal deoxynucleotidyl transferase (TdT) dUTP nick-End labeling (TUNEL) assay (green) in the control and HSu-treated animals, and in a DNase-positive control. Scale bar: 50 µm. **E**: The number of retinal ganglion cells (RGCs) was assessed with immunolabeling of the retinal sections with Brn3a (a RGC-specific marker), and Brn3a mRNA levels were evaluated with quantitative PCR (qPCR). Results are presented as the number of Brn3a-positive cells per millimeter of retina and represent the mean fold change of the control ± SEM. Scale bar: 50 µm. The qPCR results are presented as the fold change of the control retinas.

number of RGCs (Brn3a-positive cells), as well as in the Brn3a mRNA expression in HSu-treated animals compared to the controls (Figure 2E).

Undetected changes in neuronal and glial markers in the retinas of HSu-treated rats: Changes in the neural components of the retina have been described in experimental diabetes [3]. In the retinas of diabetic animals, several neuronal markers are altered [8,11,35]. However, because it is unknown whether these alterations are already present in a prediabetes state, the protein levels of neuronal marker TUJ-1 (Figure 3A) and synaptic marker synaptophysin (Figure 3B) were assessed with immunoblotting and immunohistochemistry. In the HSu model, no statistically significant changes were detected in the content and distribution of these neuronal markers (Figure 3A,B), as well as in the protein levels and distribution of the glial markers, vimentin (Figure 3C), and glial fibrillary acidic protein (GFAP; Figure 3D).

Undetected changes in proinflammatory mediators in the retina of HSu-treated rats: Increased levels of proinflammatory markers, such as inducible nitric oxide synthase isoform (iNOS) [29], TNF, and IL-1β [14,36-38], as well as activation of microglial cells [36,39], in the retina have been detected in diabetic animals and retinal cell cultures exposed to elevated glucose. The HSu diet did not statistically significantly change the transcript or protein levels of iNOS in the retina, compared with those of the age-matched controls (Figure 4A), as assessed with qPCR and western blotting, respectively. Similarly, no changes were detected in the mRNA expression and protein levels of IL-1β and TNF (Figure 4B), assessed with qPCR and ELISA, respectively.

The number of microglial cells remains unaltered in the retinas of HSu-treated rats: Microglial cell reactivity was assessed with immunohistochemistry, with retinal sections labeled for Iba1 (a general marker of microglial cells; red) and MHC-II (a marker of reactive microglia and macrophages; green). MHC-II immunoreactive cells were not detected in the retina (MHC-II-positive cells were detected only at the choroid and sclera levels; data not shown) in the control and HSu-treated animals (Figure 5A). Translocator protein (TSPO) has been used as a marker of microglia reactivity [40]. No changes were detected in the TSPO transcript levels in the retinas of the HSu-treated animals compared with those of the controls (Figure 5B). The number of Iba1-positive cells in the retinas of the HSu-treated animals was also not statistically significantly increased when compared with that of the controls. Nevertheless, there was a tendency (p=0.056) for an increase in the number of microglia in HSu retinas at the IPL and the GCL (Figure 5C).

DISCUSSION

Diet has a considerable impact in several diseases, as is the case of T2D [41]. Although many studies with rodents have shown that an HSu diet induces insulin resistance and hypertriglyceridemia [42-44], the impact of this diet on the retina remains to be clarified.

Previously, we identified molecular and cellular changes in the rat model in the heart and the brain [19,22]. In the hearts of HSu-treated rats, hypertrophy of the left ventricle was observed. Additionally, a tendency for upregulated mediators of oxidative stress, as well as angiogenesis, fibrosis, hypertrophy, and endothelial lesions, was detected [19]. In the brain, the prediabetic state results in spatial memory deficits (short- and long-term), along with changes in glucocorticoid signaling and glutamatergic neurotransmission in the hippocampus of HSu-treated animals [22]. Moreover, an HSu diet results in the upregulation of hippocampal adenosine A1 receptors and in an impairment of synaptic plasticity in the temporoammonic pathway but does not induce metabolic changes in the hippocampus [23]. These studies suggest that several changes are already present in the brain and the heart in a prediabetic state.

In this study, we evaluated for the first time the impact of the HSu diet on the retina. This study separates the effect of features of prediabetes, such as hyperinsulinemia and insulin resistance, from the bulk of systemic alterations. Understanding which cell type (neuronal, vascular, or immune) or molecular event is most sensitive to diabetes-associated metabolic alterations is a long-standing question in diabetic retinopathy [45]. The answer will help improve diagnostic approaches. The present results suggest that a 9-week HSu diet did not statistically significantly affect several parameters in the retina, which have been correlated with diabetic retinopathy, such as alterations in tight junction protein content, BRB permeability, and changes in the protein levels and mRNA expression of neural and inflammatory markers. However, the HSu diet induced a subtle but statistically significant decrease in the thickness of the inner layers of the retina, which is in accordance to the structural alterations, namely, thinning of the GCL, described in patients with diabetic retinopathy [46], and recently in prediabetic patients [47]. Nevertheless, no changes were detected in the number of RGCs and displaced amacrine cells in this layer, as well as in Brn3a mRNA levels. Moreover, no statistically significant changes were detected in neuronal markers (TUJ-1 and synaptophysin). Consistently, in the hippocampus of animals subjected to the HSu diet for 9 weeks no changes in synaptophysin were found as well [22]. However, in diabetic animals, the levels of the presynaptic marker synaptophysin are altered

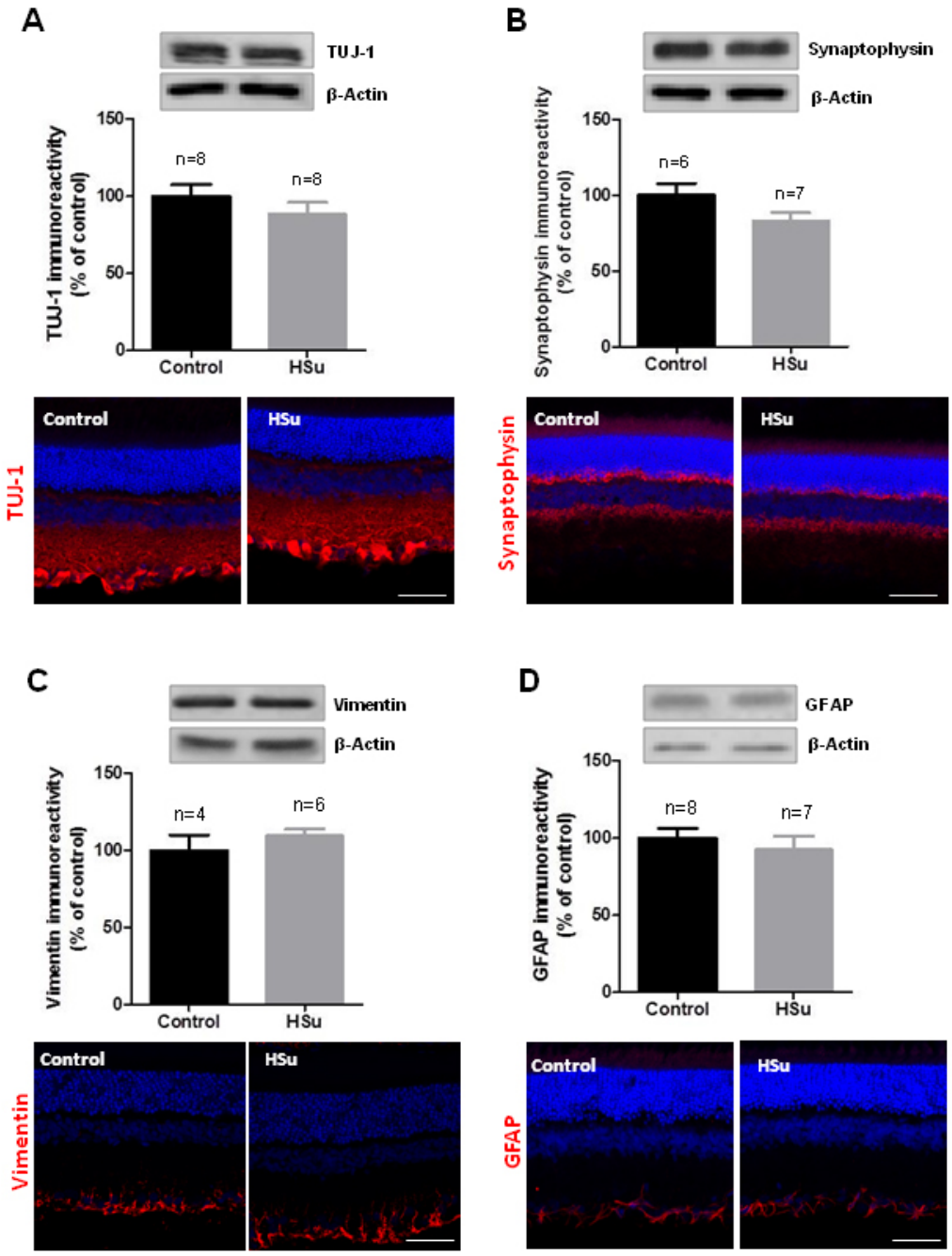

Figure 3. HSu treatment does not affect neuronal and glial markers. The neuronal markers TUJ-1 (**A**) and synaptophysin (**B**) and the glial markers vimentin (**C**) and glial fibrillary acidic protein (GFAP) (**D**) were analyzed with immunoblotting in the total retinal extracts obtained from control and high sucrose (HSu) animals. Representative images of protein immunoreactive bands are presented above the graphs, with the respective loading control (β-actin). The results are expressed as a percentage of the age-matched controls, and data are presented as mean ± standard error of the mean (SEM). Representative images from immunohistochemistry of the described proteins (red) are presented below the graphs, with 4',6-diamidino-2-phenylindole (DAPI; nuclei) staining in blue. Scale bar: 50 µm.

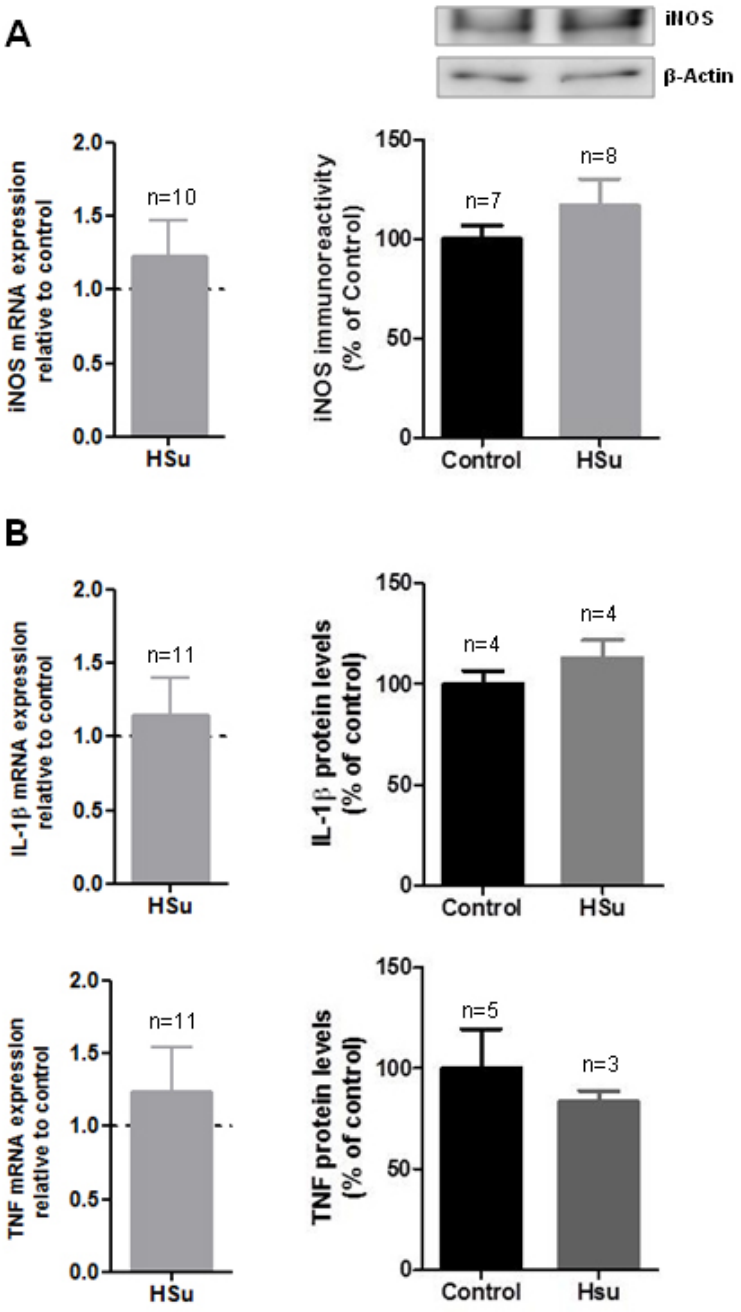

Figure 4. HSu treatment does not induce a proinflammatory state in the retina. **A**: The mRNA levels of inducible nitric oxide synthase isoform (iNOS) were assessed with quantitative PCR (qPCR). The results are presented as the mean fold change of the control ± standard error of the mean (SEM) of 10 animals. The iNOS protein levels were analyzed with western blotting. A representative image of the iNOS immunoreactive bands is presented above the graph. The results are expressed as a percentage of the age-matched controls, and data are presented as mean ± SEM of 7-8 animals. **B**: Interleukin-1 beta (IL-1β) and tumor necrosis factor (TNF) transcript and protein levels were assessed with quantitative PCR (qPCR) and enzyme-linked immunosorbent assay (ELISA), respectively. The qPCR results are presented as the mean fold change of the control ± SEM of 11 animals. The ELISA results are expressed as a percentage of the age-matched controls, and data are presented as mean ± SEM of 3-5 animals.

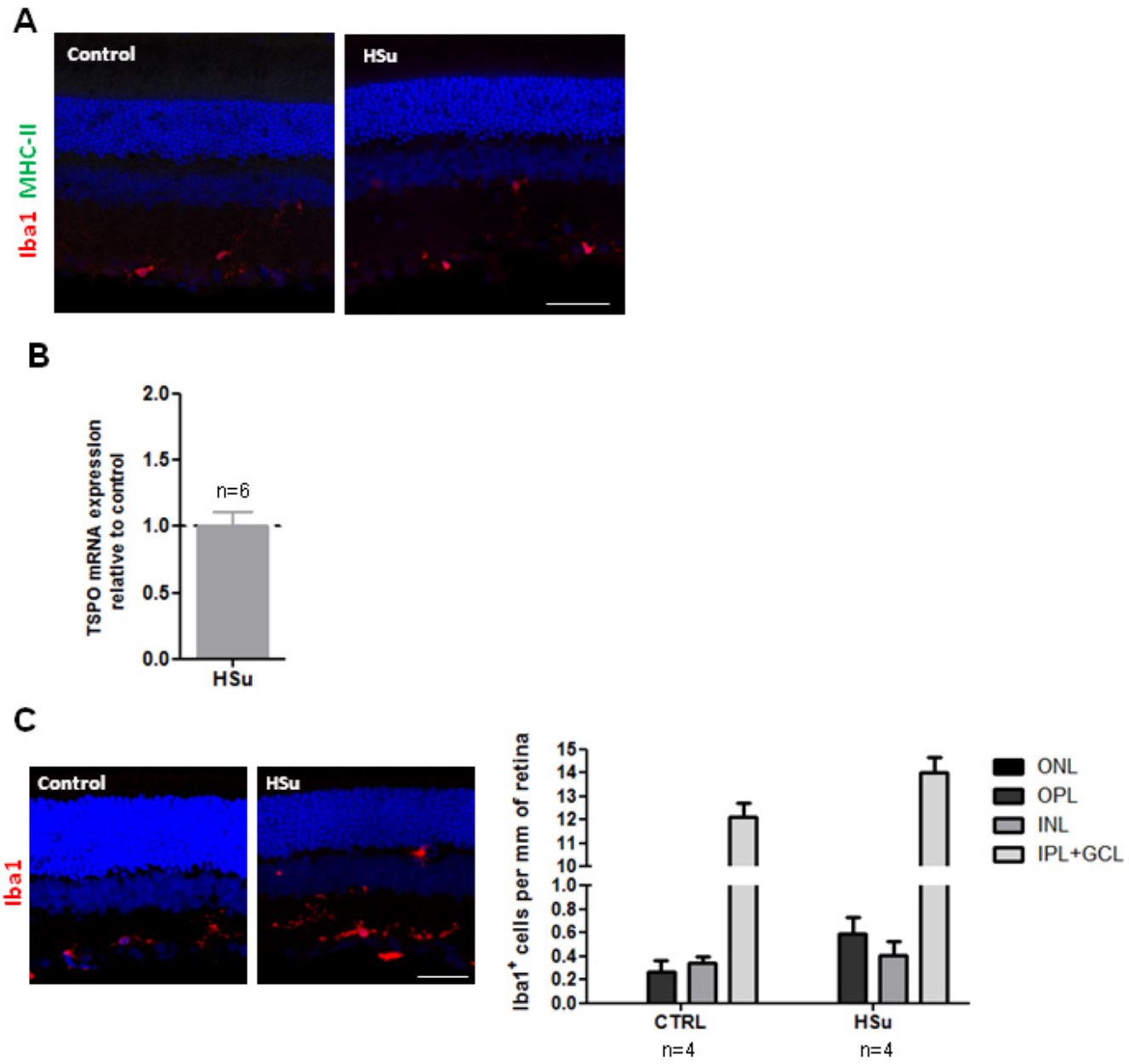

Figure 5. HSu treatment does not statistically significantly increase the number of microglial cells in the retina. **A**: Retinal sections were immunostained for microglia (Iba1; red) and for reactive microglia (MHC-II; green). Nuclei were stained with 4',6-diamidino-2-phenylindole (DAPI) ; blue). Scale bar: 50 µm. **B**: Translocator protein (TSPO; a marker of reactive microglia) transcript levels were assessed with quantitative PCR (qPCR), and results are presented as the mean fold change of the control ± standard error of the mean (SEM) of 6 animals. **C**: The number of Iba1-positive cells was counted in the retinal sections from the control and high sucrose (HSu)-treated animals. Results are presented as the number of Iba1-positive cells per millimeter of retina in each retinal layer and represent the mean ± SEM. Scale bar: 50 µm.

in the retina and hippocampus [11,35]. These data suggest that changes in synaptophysin might start occurring in the retina if the animals drink the high sucrose solution for longer periods. HSu-treated animals exhibit increased hippocampal levels of AMPA and NMDA receptor subunits, indicating some neuronal alterations already present at a prediabetic state [22].

A large body of evidence indicates that the glial marker GFAP is altered in the diabetic retina [48,49]. However, in the retinas of the HSu-treated animals, glial cells were

not reactive, based on the protein content of vimentin and GFAP. Similarly, no changes in GFAP levels were found in the hippocampus of animals subjected to the HSu diet for 9 weeks [22].

The levels of TNF, IL-1β, and iNOS remained unchanged in the retinas of the HSu-treated animals. Similar findings were reported regarding the heart and hippocampus [19,22]. The present results suggest that some cellular and structural alterations that have been associated with diabetic retinopathy [50,51] are already present in a prediabetic state. The HSu diet appears to trigger a microglial response, as we observed a tendency for the number of microglial cells to increase (proliferation) in the retina.

This tendency for an increase in the number of microglia at the IPL and the GCL may correlate with the thinning of those particular retinal layers. Although we were not able to identify neuronal apoptosis at the GCL at this prediabetic state, some neuronal stress may be already occurring triggering microglia proliferation in those layers. Whether microglia proliferation is neuroprotective or neurotoxic is an issue that remains to be clarified, in a prediabetic state or in a condition of diabetic retinopathy [52].

Although these subtle differences are already present after 9 weeks of an HSu diet, more pronounced changes might occur only after longer periods of this sucrose-enriched diet. The present results suggest that neuronal dysfunction (thinning of the inner retina) may precede or anticipate the vascular and inflammatory changes. These parameters might indicate the beginning of a pathological state, prompting the crucial relevance of a better understanding of the pathophysiological changes responsible for diabetic retinopathy in prediabetic patients. Thus, additional studies are required, which might give important clues for better prevention of diabetic retinopathy.

ACKNOWLEDGMENTS

This work was supported by Fundação para a Ciência e a Tecnologia, FCT (Portugal) and COMPETE-FEDER: Strategic Projects C/SAU/UI3282/2011–2013, PEst- UID/NEU/04539/2013, and POCI-01–0145-FEDER-007440. Centro 2020 Regional Operational Programme: HEALTHY-AGING 2020 (CENTRO-01–0145-FEDER-000012) and BRAINHEALTH 2020 (CENTRO-01–0145-FEDER-000008) also supported this work. Filipa I. Baptista, Elisa J. Campos, Raquel Boia and Maria H. Madeira acknowledge fellowships from Fundação para a Ciência e a Tecnologia, Portugal (SFRH/BPD/86830/2012, SFRH/BPD/93672/2013, PD/BD/114115/2015 and SFRH/BD/75839/2011, respectively). We would also like to thank Dr. Catarina Gomes (iCBR, Faculty of Medicine, University of Coimbra) for the useful discussions regarding this work and Timothy Fuqua for English revision. Part of manuscript data was previously presented as an oral communication at 9th Leiden International Medical Students Conference, Leiden, The Netherlands, March 11–15, 2015: Alves M.P., Boia R., Madeira M. H., Reis F., Pereira F. C., Santiago A. R., Ambrósio A. F., Baptista F. I. Prediabetes does not induce changes in tight junction proteins, neural markers and inflammatory mediators in the rat retina.

REFERENCES

1. Aiello LM. Perspectives on diabetic retinopathy. Am J Ophthalmol 2003; 136:122-35. [PMID: 12834680].
2. Cunha-Vaz J, Faria de Abreu JR, Campos AJ. Early breakdown of the blood-retinal barrier in diabetes. Br J Ophthalmol 1975; 59:649-56. [PMID: 1203221].
3. Antonetti DA, Barber AJ, Bronson SK, Freeman WM, Gardner TW, Jefferson LS, Kester M, Kimball SR, Krady JK, LaNoue KF, Norbury CC, Quinn PG, Sandirasegarane L, Simpson IA. Diabetic retinopathy: seeing beyond glucose-induced microvascular disease. Diabetes 2006; 55:2401-11. [PMID: 16936187].
4. Tang J, Kern TS. Inflammation in diabetic retinopathy. Prog Retin Eye Res 2011; 30:343-58. [PMID: 21635964].
5. Antonetti DA, Lieth E, Barber AJ, Gardner TW. Molecular mechanisms of vascular permeability in diabetic retinopathy. Semin Ophthalmol 1999; 14:240-8. [PMID: 10758225].
6. Roy MS, Gunkel RD, Podgor MJ. Color vision defects in early diabetic retinopathy. Arch Ophthalmol 1986; 104:225-8. [PMID: 3484948].
7. Daley ML, Watzke RC, Riddle MC. Early loss of blue-sensitive color vision in patients with type I diabetes. Diabetes Care 1987; 10:777-81. [PMID: 3501362].
8. Baptista FI, Gaspar JM, Cristovao A, Santos PF, Kofalvi A, Ambrosio AF. Diabetes induces early transient changes in the content of vesicular transporters and no major effects in neurotransmitter release in hippocampus and retina. Brain Res 2011; 1383:257-69. [PMID: 21281613].
9. Santiago AR, Gaspar JM, Baptista FI, Cristovao AJ, Santos PF, Kamphuis W, Ambrosio AF. Diabetes changes the levels of ionotropic glutamate receptors in the rat retina. Mol Vis 2009; 15:1620-30. [PMID: 19693289].
10. Castilho AF, Liberal JT, Baptista FI, Gaspar JM, Carvalho AL, Ambrosio AF. Elevated glucose concentration changes the content and cellular localization of AMPA receptors in the retina but not in the hippocampus. Neuroscience 2012; 219:23-32. [PMID: 22659015].
11. Gaspar JM, Baptista FI, Galvao J, Castilho AF, Cunha RA, Ambrosio AF. Diabetes differentially affects the content of exocytotic proteins in hippocampal and retinal nerve terminals. Neuroscience 2010; 169:1589-600. [PMID: 20600668].

12. Baptista FI, Pinto MJ, Elvas F, Martins T, Almeida RD, Ambrosio AF. Diabetes induces changes in KIF1A, KIF5B and dynein distribution in the rat retina: implications for axonal transport. Exp Eye Res 2014; 127:91-103. [PMID: 25064602].

13. Brucklacher RM, Patel KM, VanGuilder HD, Bixler GV, Barber AJ, Antonetti DA, Lin CM, LaNoue KF, Gardner TW, Bronson SK, Freeman WM. Whole genome assessment of the retinal response to diabetes reveals a progressive neurovascular inflammatory response. BMC Med Genomics 2008; 1:26-[PMID: 18554398].

14. Krady JK, Basu A, Allen CM, Xu Y, LaNoue KF, Gardner TW, Levison SW. Minocycline reduces proinflammatory cytokine expression, microglial activation, and caspase-3 activation in a rodent model of diabetic retinopathy. Diabetes 2005; 54:1559-65. [PMID: 15855346].

15. Zeng XX, Ng YK, Ling EA. Neuronal and microglial response in the retina of streptozotocin-induced diabetic rats. Vis Neurosci 2000; 17:463-71. [PMID: 10910112].

16. Vujosevic S, Bini S, Midena G, Berton M, Pilotto E, Midena E. Hyperreflective intraretinal spots in diabetics without and with nonproliferative diabetic retinopathy: an in vivo study using spectral domain OCT. J Diabetes Res 2013; 2013:491835-[PMID: 24386645].

17. Madeira MH, Boia R, Santos PF, Ambrosio AF, Santiago AR. Contribution of microglia-mediated neuroinflammation to retinal degenerative diseases. Mediators Inflamm 2015; 2015:673090-[PMID: 25873768].

18. Tabak AG, Herder C, Rathmann W, Brunner EJ, Kivimaki M. Prediabetes: a high-risk state for diabetes development. Lancet 2012; 379:2279-90. [PMID: 22683128].

19. Nunes S, Soares E, Fernandes J, Viana S, Carvalho E, Pereira FC, Reis F. Early cardiac changes in a rat model of prediabetes: brain natriuretic peptide overexpression seems to be the best marker. Cardiovasc Diabetol 2013; 12:44-[PMID: 23497124].

20. Diagnosis and classification of diabetes mellitus. Diabetes Care 2007; 30:Suppl 1S42-7. [PMID: 17192378].

21. Nathan DM, Davidson MB, DeFronzo RA, Heine RJ, Henry RR, Pratley R, Zinman B. Impaired fasting glucose and impaired glucose tolerance: implications for care. Diabetes Care 2007; 30:753-9. [PMID: 17327355].

22. Soares E, Prediger RD, Nunes S, Castro AA, Viana SD, Lemos C, De Souza CM, Agostinho P, Cunha RA, Carvalho E, Fontes Ribeiro CA, Reis F, Pereira FC. Spatial memory impairments in a prediabetic rat model. Neuroscience 2013; 250:565-77. [PMID: 23912035].

23. Lemos C, Rial D, Goncalves FQ, Pires J, Silva HB, Matheus FC, da Silva AC, Marques JM, Rodrigues RJ, Jarak I, Prediger RD, Reis F, Carvalho RA, Pereira FC, Cunha RA. High sucrose consumption induces memory impairment in rats associated with electrophysiological modifications but not with metabolic changes in the hippocampus. Neuroscience 2016; 315:196-205. [PMID: 26704636].

24. Boia R, Elvas F, Madeira MH, Aires ID, Rodrigues-Neves AC, Tralhao P, Szabo EC, Baqi Y, Muller CE, Tome AR, Cunha RA, Ambrosio AF, Santiago AR. Treatment with A2A receptor antagonist KW6002 and caffeine intake regulate microglia reactivity and protect retina against transient ischemic damage. Cell Death Dis 2017; 8:e3065-[PMID: 28981089].

25. Leal EC, Manivannan A, Hosoya K, Terasaki T, Cunha-Vaz J, Ambrosio AF, Forrester JV. Inducible nitric oxide synthase isoform is a key mediator of leukostasis and blood-retinal barrier breakdown in diabetic retinopathy. Invest Ophthalmol Vis Sci 2007; 48:5257-65. [PMID: 17962481].

26. Xu Q, Qaum T, Adamis AP. Sensitive blood-retinal barrier breakdown quantitation using Evans blue. Invest Ophthalmol Vis Sci 2001; 42:789-94. [PMID: 11222542].

27. Livak KJ, Schmittgen TD. Analysis of relative gene expression data using real-time quantitative PCR and the 2(-Delta Delta C(T)) Method. Methods 2001; 25:402-8. [PMID: 11846609].

28. Andersen CL, Jensen JL, Orntoft TF. Normalization of real-time quantitative reverse transcription-PCR data: a model-based variance estimation approach to identify genes suited for normalization, applied to bladder and colon cancer data sets. Cancer Res 2004; 64:5245-50. [PMID: 15289330].

29. Leal EC, Martins J, Voabil P, Liberal J, Chiavaroli C, Bauer J, Cunha-Vaz J, Ambrosio AF. Calcium dobesilate inhibits the alterations in tight junction proteins and leukocyte adhesion to retinal endothelial cells induced by diabetes. Diabetes 2010; 59:2637-45. [PMID: 20627932].

30. Goncalves A, Leal E, Paiva A, Teixeira Lemos E, Teixeira F, Ribeiro CF, Reis F, Ambrosio AF, Fernandes R. Protective effects of the dipeptidyl peptidase IV inhibitor sitagliptin in the blood-retinal barrier in a type 2 diabetes animal model. Diabetes Obes Metab 2012; 14:454-63. [PMID: 22151893].

31. Barber AJ, Antonetti DA, Kern TS, Reiter CE, Soans RS, Krady JK, Levison SW, Gardner TW, Bronson SK. The Ins2Akita mouse as a model of early retinal complications in diabetes. Invest Ophthalmol Vis Sci 2005; 46:2210-8. [PMID: 15914643].

32. Kern TS, Barber AJ. Retinal ganglion cells in diabetes. J Physiol 2008; 586:4401-8. [PMID: 18565995].

33. Barber AJ, Lieth E, Khin SA, Antonetti DA, Buchanan AG, Gardner TW. Neural apoptosis in the retina during experimental and human diabetes. Early onset and effect of insulin. J Clin Invest 1998; 102:783-91. [PMID: 9710447].

34. Nadal-Nicolas FM, Jimenez-Lopez M, Sobrado-Calvo P, Nieto-Lopez L, Canovas-Martinez I, Salinas-Navarro M, Vidal-Sanz M, Agudo M. Brn3a as a marker of retinal ganglion cells: qualitative and quantitative time course studies in naive and optic nerve-injured retinas. Invest Ophthalmol Vis Sci 2009; 50:3860-8. [PMID: 19264888].

35. VanGuilder HD, Brucklacher RM, Patel K, Ellis RW, Freeman WM, Barber AJ. Diabetes downregulates presynaptic proteins and reduces basal synapsin I phosphorylation in rat retina. Eur J Neurosci 2008; 28:1-11. [PMID: 18662330].

36. Baptista FI, Aveleira CA, Castilho AF, Ambrosio AF. Elevated Glucose and Interleukin-1beta Differentially Affect Retinal Microglial Cell Proliferation. Mediators Inflamm 2017; 2017:4316316-[PMID: 28588350].

37. Costa GN, Vindeirinho J, Cavadas C, Ambrosio AF, Santos PF. Contribution of TNF receptor 1 to retinal neural cell death induced by elevated glucose. Mol Cell Neurosci 2012; 50:113-23. [PMID: 22522145].

38. Goncalves A, Marques C, Leal E, Ribeiro CF, Reis F, Ambrosio AF, Fernandes R. Dipeptidyl peptidase-IV inhibition prevents blood-retinal barrier breakdown, inflammation and neuronal cell death in the retina of type 1 diabetic rats. Biochim Biophys Acta 2014; 1842:1454-63. [PMID: 24769045].

39. Yu Y, Chen H, Su SB. Neuroinflammatory responses in diabetic retinopathy. J Neuroinflammation 2015; 12:141-[PMID: 26245868].

40. Karlstetter M, Nothdurfter C, Aslanidis A, Moeller K, Horn F, Scholz R, Neumann H, Weber BH, Rupprecht R, Langmann T. Translocator protein (18 kDa) (TSPO) is expressed in reactive retinal microglia and modulates microglial inflammation and phagocytosis. J Neuroinflammation 2014; 11:3-[PMID: 24397957].

41. Steyn NP, Mann J, Bennett PH, Temple N, Zimmet P, Tuomilehto J, Lindstrom J, Louheranta A. Diet, nutrition and the prevention of type 2 diabetes. Public Health Nutr 2004; 7:1A147-65. [PMID: 14972058].

42. Ribeiro RT, Lautt WW, Legare DJ, Macedo MP. Insulin resistance induced by sucrose feeding in rats is due to an impairment of the hepatic parasympathetic nerves. Diabetologia 2005; 48:976-83. [PMID: 15830187].

43. Conde SV, Nunes da Silva T, Gonzalez C, Mota Carmo M, Monteiro EC, Guarino MP. Chronic caffeine intake decreases circulating catecholamines and prevents diet-induced insulin resistance and hypertension in rats. Br J Nutr 2012; 107:86-95. [PMID: 21733336].

44. Carvalho C, Cardoso S, Correia SC, Santos RX, Santos MS, Baldeiras I, Oliveira CR, Moreira PI. Metabolic alterations induced by sucrose intake and Alzheimer's disease promote similar brain mitochondrial abnormalities. Diabetes 2012; 61:1234-42. [PMID: 22427376].

45. Gardner TW, Antonetti DA, Barber AJ, LaNoue KF, Levison SW. Diabetic retinopathy: more than meets the eye. Surv Ophthalmol 2002; 47:Suppl 2S253-62. [PMID: 12507627].

46. Vujosevic S, Midena E. Retinal layers changes in human preclinical and early clinical diabetic retinopathy support early retinal neuronal and Muller cells alterations. J Diabetes Res 2013; 2013:905058-[PMID: 23841106].

47. Sahin M, Sahin A, Kilinc F, Karaalp U, Yuksel H, Ozkurt ZG, Turkcu FM, Caca I. Early detection of macular and peripapillary changes with spectralis optical coherence tomography in patients with prediabetes. Arch Physiol Biochem 2018; 124:75-9. [PMID: 28780883].

48. Feit-Leichman RA, Kinouchi R, Takeda M, Fan Z, Mohr S, Kern TS, Chen DF. Vascular damage in a mouse model of diabetic retinopathy: relation to neuronal and glial changes. Invest Ophthalmol Vis Sci 2005; 46:4281-7. [PMID: 16249509].

49. Nagayach A, Patro N, Patro I. Astrocytic and microglial response in experimentally induced diabetic rat brain. Metab Brain Dis 2014; 29:747-61. [PMID: 24833555].

50. Omri S, Behar-Cohen F, de Kozak Y, Sennlaub F, Verissimo LM, Jonet L, Savoldelli M, Omri B, Crisanti P. Microglia/macrophages migrate through retinal epithelium barrier by a transcellular route in diabetic retinopathy: role of PKCzeta in the Goto Kakizaki rat model. Am J Pathol 2011; 179:942-53. [PMID: 21712024].

51. Grigsby JG, Cardona SM, Pouw CE, Muniz A, Mendiola AS, Tsin AT, Allen DM, Cardona AE. The role of microglia in diabetic retinopathy. J Ophthalmol 2014; 2014:705783-[PMID: 25258680].

52. Altmann C, Schmidt MHH. The Role of Microglia in Diabetic Retinopathy: Inflammation, Microvasculature Defects and Neurodegeneration. Int J Mol Sci 2018; 19:[PMID: 29301251].

Articles are provided courtesy of Emory University and the Zhongshan Ophthalmic Center, Sun Yat-sen University, P.R. China. The print version of this article was created on 18 May 2018. This reflects all typographical corrections and errata to the article through that date. Details of any changes may be found in the online version of the article.